

# Attachment loss of micromechanical and nanomechanical resonators in the limits of thick and thin support structures

John A. Judge<sup>a)</sup>

*Department of Mechanical Engineering, The Catholic University of America, Washington, DC 20064*

Douglas M. Photiadis

*Naval Research Laboratory, 4555 Overlook Avenue SW, Washington, DC 20375-5320*

Joseph F. Vignola

*Department of Mechanical Engineering, The Catholic University of America, Washington, DC 20064*

Brian H. Houston and Jacek Jarzynski<sup>b)</sup>

*Naval Research Laboratory, 4555 Overlook Avenue SW, Washington, DC 20375-5320*

(Received 17 May 2006; accepted 3 October 2006; published online 11 January 2007)

Analytical expressions are provided for the energy loss from vibrating mechanical resonators into their support structures for two limiting cases: supports that can be treated as plates, and supports that act as semi-infinite elastic media, with effectively infinite thickness. The former case is applicable to many microscale resonators, while the latter is appropriate for nanoscale devices. General formulations are given, applicable to a wide range of resonator geometries. These formulations are then applied to two geometries commonly used in microelectromechanical systems and nanoelectromechanical systems applications: cantilevered beams and doubly fixed beams. Experimental data are presented to validate the finite-thickness support theory, and the predictions of the theory are also compared to data from existing literature for a microscale rectangular paddle oscillator. © 2007 American Institute of Physics. [DOI: 10.1063/1.2401271]

## I. INTRODUCTION

Loss mechanisms in microscale and nanoscale resonators have been the subject of considerable recent interest,<sup>1-5</sup> since understanding and quantifying the various sources of loss is critical for efforts to increase the overall quality factor,  $Q$ , of such devices. Resonators with high  $Q$  are desirable for a wide variety of applications, including filtering and signal processing,<sup>6-8</sup> mass sensing,<sup>9-11</sup> and atomic force microscopy,<sup>12-14</sup> among others, and pursuit of high  $Q$  is one of the principal design challenges in current research on nanoelectromechanical systems.<sup>15</sup> Energy propagation into the supporting structure is one source of loss that has received only limited attention, despite being relatively straightforward to estimate in many cases. A computational approach has been recently proposed,<sup>16</sup> but the most relevant analytic treatments appear to be those of Jimbo and Itao,<sup>17</sup> Cross and Lifshitz,<sup>18</sup> and Photiadis and Judge.<sup>19</sup>

In 1968, Jimbo and Itao<sup>17</sup> derived an expression for the energy loss from a cantilever vibrator into a semi-infinite elastic medium, by comparing the vibration energy of the cantilever with the energy associated with strain induced in the elastic medium by the shear force and bending moment at the root of the cantilever. Their result has been applied to microelectromechanical/nanoelectromechanical (MEMS/NEMS) applications in a number of later studies,<sup>1,3,4,20</sup> in which it is used to compare the order of magnitude of attachment loss to other sources, such as viscous damping and thermoelastic loss. In 2003, Cross and Lifshitz<sup>18</sup> considered

elastic wave transmission across the junction between two plates of differing widths but the same thickness, and calculated the associated energy loss.

These two studies treat the support structure to which a resonator is attached quite differently: the former considers the support to be of infinite thickness, while the latter considers the support as a plate equal in thickness to the resonator. Typically, micro- and nanoscale resonators are fabricated on substrates, or “handle-layers,” that are several orders of magnitude thicker than the devices themselves. For example, in Fig. 1, a cantilever of thickness  $h$  is shown attached to a support of greater thickness  $h_p$ . Shear (transverse) waves propagate in elastic solids at a speed  $c_s = \sqrt{E/[2(1+\nu)\rho]}$ , where  $E$  is the elastic modulus,  $\nu$  is Poisson’s ratio, and  $\rho$  is density. A resonator attached to such a solid and vibrating at frequency  $f$  will thus produce shear waves in the solid with wavelength  $\lambda_s = c_s/f$ . If the thickness of the substrate is large compared to this shear wavelength, a model in which  $h_p$  is treated as infinite can be appropriate. In many cases, however, the substrate thickness  $h_p$  is small relative to the shear wavelength, while still being much greater than the thickness  $h$  of the resonator. In this article, as in our recent Letter on cantilever attachment loss,<sup>19</sup> we consider two models of the substrate: a semi-infinite elastic medium and a plate of finite thickness. For both cases, we present general expressions for attachment loss applicable to a variety of resonator geometries, and, in the latter case, we show experimental validation of the model, representing the first experimental evidence that resonator quality factor  $Q$  can vary with substrate thickness.

For the case in which the substrate is modeled with in-

<sup>a)</sup>Electronic mail: judge@cua.edu

<sup>b)</sup>Also with SFA, Largo, MD 20774-5322.

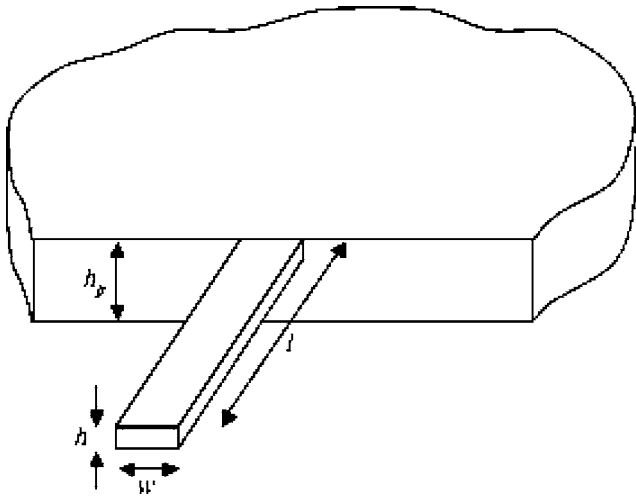


FIG. 1. A cantilever resonator attached to a support of finite thickness. The beam has length  $l$ , width  $w$ , and thickness  $h$ , and the support has thickness  $h_p$  and lateral dimensions that are assumed to be infinite. In this article, two cases are considered: a support modeled as a semi-infinite plate (finite  $h_p \geq h$ ) and a support modeled as an elastic half-space ( $h_p \rightarrow \infty$ ).

finite thickness, we follow the approach used by Jimbo and Itao.<sup>17</sup> However, in addition to being confined to the case of a cantilever beam resonator, the analysis by Jimbo and Itao assumes *plane strain*, reducing an inherently three-dimensional problem to two dimensions. All wave propagation in the elastic half-space thus takes the form of plane waves, and the width of the cantilever is not present in the analysis: in essence, the assumption is one of *infinite* cantilever width. Indeed, the results derived in Ref. 17 for normal and shear loads on the surface of the elastic half-space are equivalent to the solutions presented by Miller and Pursey<sup>21</sup> for normal and transverse vibrations of an infinitely long, finite-width strip on the surface of a semi-infinite solid. The model presented here considers the full three-dimensional problem and can be applied to a variety of resonator geometries.

For the case of a support of finite thickness, we consider a semi-infinite plate with a thickness that need not be the same as that of the resonator itself. Using the plate-edge admittance results first reported by Eichler,<sup>22</sup> we derive expressions for resonator attachment loss, which again are applicable to a variety of resonator geometries. For the case in which the plate thickness is equal to the resonator thickness, the expressions agree qualitatively with those of Cross and Lifshitz.<sup>18</sup>

The purpose of this article is thus to provide accurate analytical expressions for the energy loss from finite-width resonators into their support structures, in the limits of thick and thin support structures, and to report experimental data that validate the latter model. In Secs. II A and II B, we show expressions for energy loss in terms of forces and moments developed at the resonator attachment point, for semi-infinite solid and finite-thickness plate models of the support, respectively. In Sec. III, we apply the results of Secs. II A and II B to two specific geometries commonly used as MEMS and NEMS oscillators: cantilevered beams and doubly fixed beams. For both geometries, we present experimental data on

a series of macroscale beams to validate the finite-thickness support theory. We also compare predictions to data from the recent literature for a third resonator configuration, a microscale rectangular paddle, for which experimental measurements suggest that attachment loss may be a dominant loss mechanism at low temperature.<sup>23</sup> Finally, in Sec. IV, we conclude by comparing the results of the two models of the support structure, and commenting on their utility in various regimes of resonator geometry.

## II. POWER FLOW INTO SUPPORT STRUCTURES

The energy lost from a vibrating resonator into the surrounding structure consists of the net work done by the resonator at the point of attachment. We restrict our attention to cases in which the dimensions of the point of attachment are small compared to the vibration wavelengths in the substrate at the resonant frequency of the device. In such cases, the effects of the vibrating resonator on the substrate can be modeled as harmonic point forces and moments acting at the attachment point. If  $\mathbf{F}$  is a vector of these point loads, and  $\mathbf{v}$  is the corresponding vector of the harmonic linear and angular velocities at that point, then the average power transmitted to the support is simply<sup>24</sup>

$$\Pi = \frac{1}{2} \text{Re}(\mathbf{F} \cdot \mathbf{v}). \quad (1)$$

Here, the forces in the vector  $\mathbf{F}$  are multiplied by linear velocities in  $\mathbf{v}$ , while the moments in  $\mathbf{F}$  are multiplied by the angular velocities in  $\mathbf{v}$ , giving consistent units for power. The amplitude of all forces and moments are taken to be real; the resulting deformations may be complex, but only the real portions of the velocities (or imaginary parts of displacements) are needed to calculate the energy lost to the support structure and not recovered.

### A. Flow into semi-infinite support

For a support structure modeled as a semi-infinite elastic medium, the load vector  $\mathbf{F}$  contains various forces and moments applied at a single point on the surface of the half-space (the point of attachment of the resonator).  $\mathbf{F}$  can consist of four types of loading in general: forces normal to the support surface, forces parallel to the surface, moments about an axis parallel to the surface, and moments about the axis normal to the surface. We refer to these, respectively, as normal force  $F_n$ , shear force  $F_s$ , bending moment  $M_b$ , and torsional moment  $M_t$ , and consider each to be harmonic with frequency  $\omega$ , so that, for example,  $F_n = |F_n|e^{i\omega t}$ . The velocity vector  $\mathbf{v}$  consists of the time-rate-of-change of the corresponding linear and angular displacements: displacement  $w$  normal to the surface, displacement  $u$  parallel to the surface, rotation  $\theta$  out of the plane of the surface, and rotation  $\phi$  within the surface plane. Note that the significance of each load type depends upon the specific resonator geometry. For example, in the case of a beam cantilevered normal to the surface and vibrating in its fundamental flexural mode, a shear force and bending moment are developed at the attach-

ment point, but normal loads on the surface due to axial motion of the beam are negligible to first order, and torsional motion is not present.

Miller and Pursey<sup>21</sup> consider two load conditions on the surface of a semi-infinite medium. In both cases the condition is not a point load but is instead a stress distribution over a circle of finite radius. The first case is a circular area over which the stress is constant and directed normal to the surface of the half-space; this reduces to a normal point force in the limit of zero radius. The second case is a circular area over which the load is a shear stress directed along the surface and circumferentially around the circle, with a magnitude proportional to the distance from the circle's center. This case represents a torsional load, and reduces to an applied torsional point moment in the zero radius limit.

Bycroft<sup>25</sup> considers the vibration induced in a semi-infinite elastic solid by motion of a rigid circular plate attached to its surface, and calculates the impedance with respect to all four possible loading conditions. Unlike Miller and Pursey, who specify the stress distribution on the surface of the half-space, Bycroft specifies the boundary condition that the surface displacement must match that of the rigid plate. However, in the limit of zero radius, these results collapse to represent point forces or moments, and, in the two cases considered by Miller and Pursey, agree with those results.

Following the derivations by Miller and Pursey<sup>21</sup> and Bycroft,<sup>25</sup> and considering each load in isolation, the linear and angular displacements at the resonator attachment point are as follows:

$$w = \frac{F_n k_s}{2G\pi\tau} \int_0^\infty \frac{k\sqrt{k^2-1}}{N_0(k)} dk, \quad (2)$$

$$u = \frac{F_s k_s}{4G\pi} \int_0^\infty \left( \frac{k^3}{\sqrt{k^2-\tau^2}} - \frac{k^3-2k}{\sqrt{k^2-1}} \right) dk, \quad (3)$$

$$\theta = \frac{M_b k_s^3 \tau}{4G\pi} \int_0^\infty \frac{k^3 \sqrt{k^2-1}}{N_0(k)} dk, \quad (4)$$

$$\phi = \frac{M_t k_s^3}{8G\pi} \int_0^\infty \frac{k^3}{\sqrt{k^2-1}} dk, \quad (5)$$

where

$$N_0(k) = 4k^2 \sqrt{1-k^2} \sqrt{1/\tau^2 - k^2} + (2k^2 - 1/\tau^2)^2,$$

$G$  is the shear modulus (modulus of rigidity) of the material {given by  $E/[2(1+\nu)]$ },  $k_l$  and  $k_s$  are the longitudinal and shear wave numbers in the solid at frequency  $\omega$ ,  $\tau$  is their ratio ( $k_l/k_s$ ), and  $k$  has been normalized by  $k_l$  in Eqs. (2) and (4) and by  $k_s$  in Eqs. (3) and (5), so that the integrals are dimensionless.

The integrals in Eqs. (3) and (5) can be solved in closed form, and since only the imaginary part is required, the integration can be limited to the ranges 0 to  $\tau$  for the first term of Eq. (3), and 0 to 1 for the second term and for Eq. (5). The

results for the two integrals are  $(-2\tau^3/3-4/3)i$  and  $(-2/3)i$ , respectively. If each load case is considered in isolation, the average power delivered to the support is

$$\Pi_{F_s} = (0.0265\tau^3 + 0.0531)\omega \frac{F_s^2 k_s}{G}, \quad (6)$$

$$\Pi_{M_t} = 0.0133\omega \frac{M_t^2 k_s^3}{G}. \quad (7)$$

The integrals in Eqs. (2) and (4) can be solved numerically for particular values of  $\tau$ , although there is a pole in the real part, the imaginary part remains bounded. For  $\tau^2=1/3$  (corresponding to Poisson's ratio  $\nu=1/4$ ), the resulting power is

$$\Pi_{F_n} = 0.00911\omega \frac{F_n^2 k_s}{G}, \quad (8)$$

$$\Pi_{M_b} = 0.00473\omega \frac{M_b^2 k_s^3}{G}. \quad (9)$$

The result for applied moment  $M_b$  can be achieved either by considering Bycroft's result for rotation about an axis parallel to the surface (in the limit of zero plate radius) or by superposing two solutions to the problem of applied normal force, 180° out of phase temporally and a short distance apart spatially, and taking the limit as the distance between the forces approaches zero.

Note that the expressions given in Eqs. (6) and (9) are valid when each load case is considered in isolation. There also exist cross terms that relate shear force  $F_s$  to rotation  $\theta$ , and bending moment  $M_b$  to displacement  $u$ ; these contribute to the total power delivered in the form of a term proportional to the product of  $F_s$  and  $M_b$ . However, here we neglect these cross terms, under the assumption that, for most resonator geometries, a single load type will be responsible for most of the energy loss into the support, and the loss resulting from other loads and from the cross terms will be negligible.

Equations (6) and (9) show that the energy lost per cycle of oscillation,  $\Delta U$  (which is  $2\pi\Pi/\omega$ ) depends directly on shear wave number  $k_s$  in the case of applied forces and on  $k_s^3$  in the case of applied moments. It is important to recall, however, that the forces and/or moments developed at the attachment of the resonator depend on the resonator geometry and scale; thus, there is a further dependence of energy loss on wave number indirectly through the scaling of that force or moment. Furthermore, to determine a loss factor (or its reciprocal, quality factor  $Q$ ) for any oscillator, the energy lost must be compared to the energy remaining in the oscillator, which itself depends on the geometry of the oscillator in question. Thus, any conclusions about the scaling of loss factor with wave number (or frequency) require consideration of the nature of the specific oscillator in question. As examples, we describe the loss from cantilevered beams, doubly clamped beams, and rectangular paddle oscillators in Sec. III.

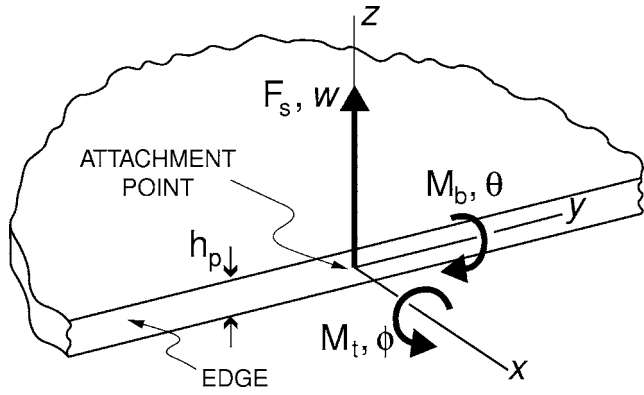


FIG. 2. Semi-infinite plate geometry. Note that, assuming small angles, the bending rotation  $\theta = -dw/dx$ , while torsional rotation  $\phi = dw/dy$ .

### B. Flow into plate edge

If the support structure is modeled as a plate, the energy loss can be found by considering the response of the plate to loads applied to its edge. The admittance at the edge of a semi-infinite plate was first formulated in integral form in 1964 by Eichler,<sup>22</sup> whose approximations of the solutions were refined by Kaufmann,<sup>26</sup> these integrals have recently been solved in closed form by Su and Moorhouse.<sup>27</sup> We consider shear forces normal to the plate,  $F_s$ , bending moments about the axis parallel to the plate edge,  $M_b$ , and torsional moments about the axis perpendicular to the plate edge,  $M_t$ , as shown in Fig. 2. Note that three other loads, not considered in Ref. 27 or in the present work, are also possible: forces normal to the plate edge, shear forces parallel to the plate, and bending moments about the axis perpendicular to the plate. The stiffness of the plate with respect to any of these latter three loads is much greater than the stiffness with respect to the former three, and, for most resonator geometries, attachment loss due to the latter can be assumed to be negligible compared to loss due to the three load conditions considered here.

The point mobility matrix  $Y$  relates the normal angular velocity,  $\Omega_n$ , the tangential angular velocity  $\Omega_t$ , and the transverse linear velocity,  $V_z$ , of the attachment point to the applied loads by the expression

$$\begin{bmatrix} \Omega_n \\ \Omega_t \\ V_z \end{bmatrix} = i\omega \begin{bmatrix} \theta \\ \phi \\ w \end{bmatrix} = \frac{1}{\sqrt{\rho_p h_p D}} [Y] \begin{bmatrix} M_t \\ M_b \\ F_s \end{bmatrix},$$

$$Y = \begin{bmatrix} y_{11}k^2 & 0 & 0 \\ 0 & y_{22}k^2 & y_{23}k \\ 0 & y_{32}k & y_{33} \end{bmatrix}, \quad (10)$$

in which  $\rho_p$  is the plate density,  $h_p$  is its thickness, and  $D = Eh_p^3/12(1-\nu^2)$  is its stiffness.

For the case  $\nu=0.3$ , Su and Moorhouse<sup>27</sup> give  $\text{Re}(y_{11}) = \text{Re}(y_{22}) = 0.21645$ ,  $\text{Re}(y_{23}) = \text{Re}(y_{32}) = -0.29149$ , and  $\text{Re}(y_{33}) = 0.46198$ . The resulting expressions for power radiated into the plate are

$$\Pi_{F_s} = 0.763 \frac{F_s^2}{h_p^2 \sqrt{E\rho_p}}, \quad (11)$$

$$\Pi_{M_{b/t}} = 1.182 \frac{\omega M_{b/t}^2}{h_p^3 E}, \quad (12)$$

when each load is again considered in isolation [note that Eq. (12) applies for both bending moment and torsional moment load conditions].

If both bending moment and shear force are present, the off-diagonal terms of  $Y$  result in an additional contribution such that the total power is

$$\Pi_{F_s \text{ and } M_b} = \Pi_{F_s} + \Pi_{M_b} - 1.751 \frac{\sqrt{\omega} M_b F_s}{\rho^{1/4} h^{5/2} E^{3/4}}. \quad (13)$$

Note that, unlike the case of the semi-infinite support model, the cross terms are not neglected for the case of the plate model, since, for a sufficiently thin plate, the contribution to power flow from all three terms in Eq. (13) may be of similar order.

## III. LOSS FROM OSCILLATORS (CASE STUDIES)

Two oscillator geometries commonly used in MEMS and NEMS applications, cantilevered beams and doubly fixed beams, were considered in detail to determine attachment energy loss. For each of these case studies, macroscale experiments were conducted to validate the thin-plate limit theory presented in Sec. II B. In addition, attachment loss calculations were carried out numerically for a doubly supported rectangular plate oscillator design, for which measured values of  $Q$  reported in the literature appear to approach the limit imposed by attachment loss.

### A. Cantilevered beam oscillators

#### 1. Prediction of cantilever attachment loss

The quality factor,  $Q$ , of an oscillator is a measure of the ratio of the energy of vibration of the oscillator to the energy lost;<sup>28</sup> the reciprocal of  $Q$  is the loss factor  $\delta$ ,

$$\delta = \frac{1}{Q} = \frac{\Delta U}{2\pi U} = \frac{\Pi}{\omega U}, \quad (14)$$

where  $\Delta U$  is the total energy lost per cycle of oscillation, due to all applicable loss mechanisms, and  $\Pi$  is the total net power flow out of the oscillator. The loss factor due to attachment to the support,  $\delta_{\text{attach}}$ , can be found by replacing the total power  $\Pi$  with the power flowing to the support (derived in Secs. II A and II B). This sets an upper bound on the oscillator quality factor: if support loss is dominant and all other loss mechanisms are neglected,  $Q \approx Q_{\text{attach}} = \delta_{\text{attach}}^{-1}$ .

The resonant behavior of a cantilevered beam oscillator fixed at its root is well known.<sup>29</sup> The energy of vibration in the  $n$ th mode can be written as  $U_n = 1/2 \rho w h l \omega_n^2 u_0^2$ , where  $\rho$  is the density,  $\omega_n$  is the resonant frequency of the mode, and the cantilever has length  $l$ , width  $w$ , and thickness  $h$ . This energy is scaled by  $u_0$ , the arbitrary amplitude of the free vibration mode shape, as are the shear force and bending moment developed at the cantilever root,

$$F_s = 2EI k_n^3 \beta_n u_0, \quad (15)$$

$$M_b = -2EI k_n^2 u_0, \quad (16)$$

where

$$\beta_n = \frac{\sinh(k_n l) - \sin(k_n l)}{\cosh(k_n l) + \cos(k_n l)},$$

$E$  is Young's modulus, and  $I = wh^3/12$  is the moment of inertia of the beam. The eigenvalues are  $k_n l = \{1.875, 4.694, \dots\}$ , determined from  $\cosh(k_n l)\cos(k_n l) = -1$ , and are related to the resonant frequency by  $\omega_n = k_n^2 \sqrt{EI/\rho wh}$ .

In reality, the cantilever is *not* fixed at its root, but is instead attached to a support structure that has finite stiffness. However, if the stiffness of the support is sufficiently high, the shear force and bending moment derived using the above assumption are an accurate approximation of the true load on the support. For the case of a support modeled as a half-space, the contribution to radiated power due to bending moment is negligible compared to the contribution due to shear force, and the loss factor can be determined simply by substituting Eq. (15) into Eq. (6) and the resulting expression into Eq. (14). For the fundamental beam vibration mode, with cantilever and support made from the same material, the result is

$$Q^{-1} = A \frac{w}{l} \left( \frac{h}{l} \right)^4, \quad (17)$$

where the numerical coefficient  $A$  is a weak function of Poisson's ratio,  $\nu$ , and is 0.31 for  $\nu=0.3$  and 0.29 for  $\nu=0.25$ . Note that this expression differs substantially from that given by Ref. 17, in which  $Q^{-1}$  is proportional only to  $(h/l)^3$  when the bending moment contribution is neglected, and does not depend on the cantilever width  $w$ .

In the case of a support modeled as a plate, the radiated power can be found by substituting Eq. (15) and Eq. (16) into Eq. (13), and the attachment loss factor is found to be

$$Q^{-1} = \frac{w}{l} \left[ A_1 \left( \frac{h}{h_p} \right)^2 + A_2 \left( \frac{h}{h_p} \right)^{5/2} + A_3 \left( \frac{h}{h_p} \right)^3 \right], \quad (18)$$

where  $A_1$ ,  $A_2$ , and  $A_3$  are weak functions of Poisson's ratio,  $\nu$ . For  $\nu=0.3$ , the coefficients are  $A_1=0.95$ ,  $A_2=-0.65$ , and  $A_3=0.24$ . The first term is due to shear force  $F_s$  at the cantilever attachment, the third is due to bending moment  $M_b$ , and the second is the cross term arising from the off-diagonal elements of the  $Y$  matrix and depending on both  $F_s$  and  $M_b$ . It can be seen from Eq. (18) that, for any case in which  $h_p$  is large relative to  $h$ , the shear force term dominates and the effect of the bending moment at the attachment point may be neglected.

The predicted values of attachment loss due are independent of scale and depend only on relative dimensions: the results for loss into a half-space depend only on the beam aspect ratios  $h/L$  and  $w/L$ , while the results for loss into a plate edge depend also on the ratio of beam to plate thicknesses,  $h/h_p$ . In either case, the greatest source of attachment loss is that due to shear force developed at the oscillator attachment.

The error introduced by the use of shear force  $F_s$  and bending moment  $M_b$  corresponding to a cantilever with fixed

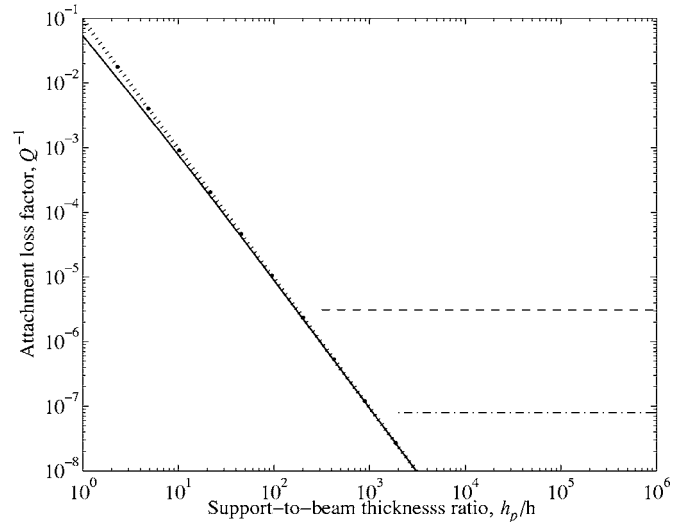


FIG. 3. Attachment loss from a cantilevered beam resonator vibrating in its fundamental flexural mode, as a function of ratio of support plate thickness  $h_p$  to cantilever thickness  $h$ . Four curves are shown: (—) prediction for support modeled as a thin plate, Eq. (18), applicable when  $h_p \ll \lambda_p$ , (···) first term of Eq. (18) only, and two predictions for thick support structure, Eq. (17), applicable when  $h_p \gg \lambda_p$ ; (---) asymptote for  $h/l=1/10$  and (-·-) asymptote for  $h/l=1/25$ . The curves shown are for the case  $w/l=1/10$ ; all predictions scale linearly with  $w/l$ .

root is negligible for the case of an infinite-thickness support, and is also negligible for a finite-thickness support as long as the support thickness is several times larger than the cantilever thickness. Even for cases in which the support thickness is the same as the cantilever thickness, the result provides a valid estimate of the order of magnitude of attachment loss. Cross and Lifshitz,<sup>18</sup> in their consideration of energy flow from a narrow plate to a wider plate of equal thickness, make an analogous approximation: the behavior of the narrow plate is first solved using the assumption of zero displacement at the boundary, then the radiation into the wider plate is calculated from the resulting strain at the point of attachment.

A more accurate calculation of loss into a thin support requires the cantilever behavior to be solved using a mixed boundary condition at the root: the condition ( $w=0, dw/dx=0$ ) is replaced by a relationship between  $w$ ,  $dw/dx$ ,  $d^2w/dx^2$ , and  $d^3w/dx^3$  determined by considering the second and third rows of Eq. (10) and noting that  $F_s = EI(d^3w/dx^3)$  and  $M_b = EI(d^2w/dx^2)$ . The resulting problem can be solved numerically; the result indicates that the error introduced by the rigid-attachment approximation is roughly a factor of 2 when the cantilever and plate are of equal thickness, and less than 10% when the plate thickness is twice that of the cantilever.

A plot of attachment loss from a cantilevered beam resonator vibrating in its fundamental flexural mode is shown in Fig. 3. Four curves are shown relating the loss factor,  $Q^{-1}$ , to the thickness of the support plate  $h_p$ , scaled by the cantilever thickness  $h$ . The first is the prediction for attachment loss achieved by modeling the support as a thin plate [based on Eq. (18)]. The second is an approximate version of the same prediction, in which contributions from bending moment and rotation of the attachment point are neglected, and the loss is

TABLE I. Geometry, predicted  $Q$ , and measured  $Q$  for cantilevered beams.

Plate	Beam	Dimensions (mm)			Aspect ratios			Predictions				Measurements		
		Length $l$	Width $w$	Thickness $h$	$l/w$	$l/h$	$h_p/h$	Freq. (Hz)	$Q_{\text{attach}}$	$Q_{\text{visc}}$	$Q_{\text{ac}}$	$Q_{\text{total}}$	Freq. (Hz)	$Q$
1	1	9.53	1.27	0.61	7.5	15.6	20.8	5523.8	3974	16000	5244	1193	5649	1123
	2	19.05	2.54	1.09	7.5	17.4	11.6	2934.5	940	25000	5920	622	2641	360
	3	19.05	3.81	1.14	5.0	16.7	11.1	2934.5	627	25000	3927	450	2669	303
	4	12.70	1.70	1.12	7.5	11.4	11.4	5696.5	1238	30000	4465	715	5045	809
2	5	9.53	1.27	0.71	7.5	13.4	13.4	6444.5	1702	20000	7137	900	6598	654
	6	19.05	2.54	1.19	7.5	16.0	8.0	2704.4	637	22000	5028	465	2533	306
	7	19.05	3.81	1.22	5.0	15.6	7.8	2761.9	408	22000	3479	321	2548	275
	8	9.53	1.70	0.71	5.6	13.4	13.4	6444.5	1277	20000	12606	803	6782	552
3	9	9.53	1.27	0.64	7.5	15.0	7.5	5754.0	567	17000	6154	429	5908	271
	10	19.05	2.54	1.27	7.5	15.0	3.8	2934.5	155	25000	5920	139	3018	52
4	11	9.53	1.27	0.61	7.5	15.6	2.6	5523.8	79.6	16000	5244	76.0	6496	12
	12	19.05	2.54	1.37	7.5	13.9	1.2	3107.2	18.2	27000	6637	18.0	2490	2.9
	13	23.75	3.18	1.55	7.5	15.3	1.0	2258.4	14.5	26000	5449	14.4	1658	2.4

a linear function of the square of beam aspect ratio [the first term of Eq. (18)]. This curve only differs significantly from the first for cases in which the support thickness is less than an order of magnitude greater than the cantilever thickness, and shows that even for such cases, the simple linear relationship provides a good order-of-magnitude estimate of loss. The final two curves depict the infinite-thickness asymptotes based on the half-space support model of Eq. (17), for two different cantilever thickness-to-length ratios  $h/l$ . Although strictly accurate only in the infinite  $h_p$  limit, these curves provide a valid order-of-magnitude estimation of attachment loss for any case in which the support thickness is large compared to the shear wavelength in the support at the frequency of interest. The speed of shear waves in an elastic solid,  $c_s = \sqrt{E/[2(1+\nu)\rho]}$ , is a function of elastic modulus  $E$ , density  $\rho$ , and Poisson's ratio  $\nu$ . At the fundamental resonant frequency  $f$  of a cantilever (which depends on  $E$  and  $\rho$  as well as cantilever dimensions), the shear wavelength  $\lambda_s = c_s/f$  is between  $3.5l^2/h$  and  $4.0l^2/h$  for Poisson's ratio,  $\nu$ , between 0.2 and 0.5. Thus, the support thickness must be many times greater than the length of the cantilever for the half-space support model to be applicable. Many MEMS and nanoscale devices are fabricated on wafers with thickness less than 1 mm: in such cases, MEMS cantilevers with lengths of tens or hundreds of micrometers (megahertz frequencies) will fall in the regime governed by the plate model, while nanoscale cantilevers, with lengths near or below 1  $\mu\text{m}$  and frequencies of hundreds of megahertz or gigahertz, will be in the half-space model regime.

## 2. Experimental measurement of cantilever attachment loss

Experimentally validating the half-space support model of Sec. II A is quite difficult: for nanoscale devices, in which wafer thickness may be relatively great enough that the support acts as a half-space, loss factors due to other loss mechanisms are typically much greater than the extremely small values predicted for attachment loss. Validation of the plate support model, by contrast, is possible using a macroscale

experiment. At macroscale beams can easily be fabricated from plates monolithically with a wide range of dimensions. Of particular importance is the relative thickness of the beam to the plate, which is somewhat impractical to specify with MEMS fabrication. Furthermore, other dissipation mechanisms such as the surface adsorption of organic compounds, which are difficult to control in microscale systems, are not a factor for macroscale experiments.

A series of cantilevers were milled from the edges of large aluminum plates of varying thickness. Table I shows the specific dimensions used, as well as beam aspect ratios and the ratio of plate to beam thicknesses. The plates, roughly 2 ft. square, were in all cases several times larger than the plate flexural wavelength at the frequency of the cantilevers' fundamental vibration mode. The half of each plate furthest from the cantilever being measured was coated with viscoelastic damping material to minimize reflection of energy-carrying elastic waves from the boundaries. The lower quarter of the plate is buried in sand, which further minimizes reflections (see Fig. 4).

Excitation was provided electrostatically by grounding the support plate and applying a drive voltage to an electrode a short distance from the tip of the cantilever to be measured. The force applied to the cantilever is

$$F = \frac{2A\epsilon_0}{d^2} V_{\text{dc}} V_{\text{ac}}, \quad (19)$$

where  $\epsilon_0$  is the permittivity of free space,  $d$  is the size of the gap between electrode and cantilever,  $A$  is the area of overlap,  $V_{\text{dc}}$  is the dc component of the applied voltage, and  $V_{\text{ac}}$  is the component of voltage oscillating at the drive frequency. The vibration response of the cantilevers was measured using a laser vibrometer. The vibrometer, which measures only the component of velocity along the line of sight, was mounted on a tripod and oriented to monitor the out-of-plane motion of the cantilevers. Adequate signal-to-noise conditions existed for  $V_{\text{dc}} \approx 50 \text{ V}$  and  $|V_{\text{ac}}| \approx 50 \text{ V}$ , for gap  $d$  as large as 1 mm.

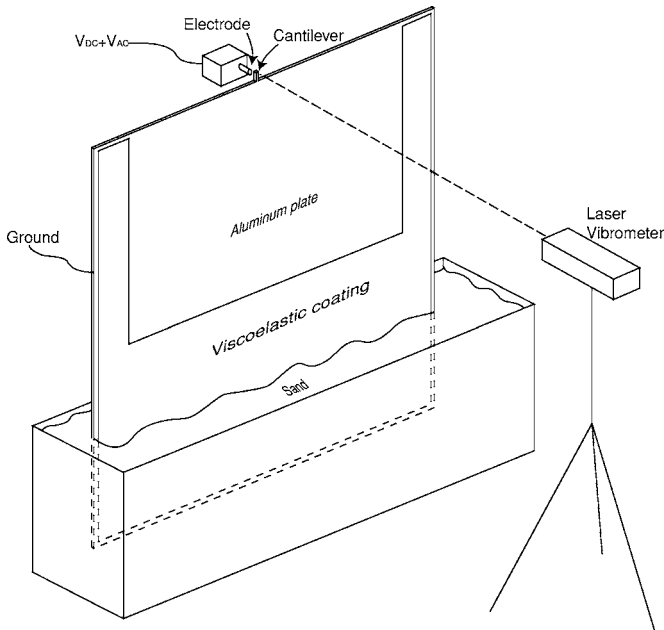


FIG. 4. Experimental setup.

The fundamental resonant frequency of each cantilever was found by applying the drive voltage continuously and sweeping the frequency of the ac component with the vibrometer trained on the tip of that cantilever. Cantilever quality factors,  $Q$ , were obtained by measuring the half-power bandwidths in the frequency spectra of the response. For beams with sufficiently high  $Q$  (specifically, beams 1–9), the values obtained via frequency sweep were confirmed by measuring the time-domain decay rate of free vibration; the results matched the frequency sweep measurements to within 10% for all cases. To prevent squeeze-film damping<sup>30</sup> (a dissipation mechanism associated with the fluid-filled gap between a planar vibrator and a stationary surface) from limiting  $Q$  in these measurements, preliminary frequency sweeps with different gaps  $d$  were conducted. Because drive force, and thus beam tip velocity, increases with decreasing gap  $d$ , the optimal gap is the smallest gap  $d$  for which squeeze-film damping is negligible. For each beam, this was found by repeating the frequency sweep with ever-decreasing gaps and noting the distance at which squeeze-film damping begins to cause measurable decreases in  $Q$ .

Vibrometer scans of the entire surface of each cantilever confirmed that the measured resonant peaks corresponded to motion in the fundamental flexural mode of the cantilevers. In addition, several scans were performed over large areas of the support plates, both before and after the application of the viscoelastic material and the placement in sand. These measurements showed a dramatic decrease in the standing-wave ratio of the plate vibration due to the sand and viscoelastic material, indicating that these treatments were successful in minimizing the amount of the energy reflected from the plate boundaries. We estimate that, at the attachment point of the cantilevers, the amplitude of flexural waves returning from the plate was no more than 15% of the amplitude of outgoing waves. For a truly semi-infinite plate

there would be no returning waves, and the vibration at the cantilever root would be solely due to outgoing waves radiating into the plate.

The measured quality factors are compared to theoretical predictions based on Eq. (18) in Table I. Because the measured  $Q$  values are the quality factors due to the combined action of all loss mechanisms, they must be compared to predictions that incorporate not only attachment loss but also estimates of any other significant sources of loss in the experiment. As noted above, many sources of loss that are relevant at micro- and nanoscales can be safely neglected at the macroscale. However, the experiment was conducted in air, so the contributions of viscous and acoustic loss must be considered, as well as the intrinsic loss of the aluminum material. Estimates of these losses are included in Table I, as well as the total  $Q$ , found from  $1/Q_{\text{total}} = 1/Q_{\text{attach}} + 1/Q_{\text{visc}} + 1/Q_{\text{ac}} + 1/Q_{\text{int}}$ .

Intrinsic loss in aluminum is known to vary widely with alloy and processing history; here, the intrinsic loss of aluminum,  $Q_{\text{int}}$ , is taken to be 3000. The estimates of viscous and acoustic losses were obtained using expressions given by Vignola *et al.*<sup>31</sup> The expression for viscous loss is

$$Q_{\text{visc}} = \frac{h\rho_s}{3} \sqrt{\frac{\omega}{2\eta\rho}}, \quad (20)$$

where  $\rho_s$  is the density of the device,  $\omega$  is the resonance frequency, and  $\eta$  and  $\rho$  are the viscosity and density of the surrounding fluid, respectively. This expression is based on a model proposed originally by Kokubun *et al.*<sup>32,33</sup> and first applied to cantilevers by Blom *et al.*,<sup>34</sup> in which the structure is modeled as a collection of spheres. Acoustic loss is estimated from the expression

$$Q_{\text{ac}} = \frac{\omega\rho_s h}{2\sigma_r \rho c}, \quad (21)$$

where  $c$  is the sound speed of the medium and  $\sigma_r$  is the radiation efficiency, defined as the ratio of the average acoustic power radiated per unit area of the vibrating structure to the acoustic power radiated per unit area by a uniformly vibrating, circular piston.<sup>35</sup> The radiated power from a baffled planar oscillator is given by Williams;<sup>36</sup> note that edge effects have been neglected.

The measured values of  $Q$  shown in Table I show the same general trend as the predicted values of  $Q_{\text{total}}$ ; they are lower than the predictions in all cases and are within a factor of 2 for all cases except beams 10–13; these are the beams with the lowest  $Q$ , indicating that a significant amount of vibration energy is radiated into the attachment. The assumption that the finite support plate acts as a semi-infinite plate is least valid for these cases, in which plate flexural waves reflected from the boundaries have significant amplitude relative to the vibration of the cantilevers themselves. Thus, the predictions are based on the assumption of a plate which has significantly less vibration amplitude at the attachment point than the cases actually measured, resulting in an overprediction of  $Q_{\text{attach}}$ . The measured data are also shown graphically in Fig. 5 alongside the prediction of attachment loss factor (scaled by aspect ratio  $w/l$ ). Note that it is not

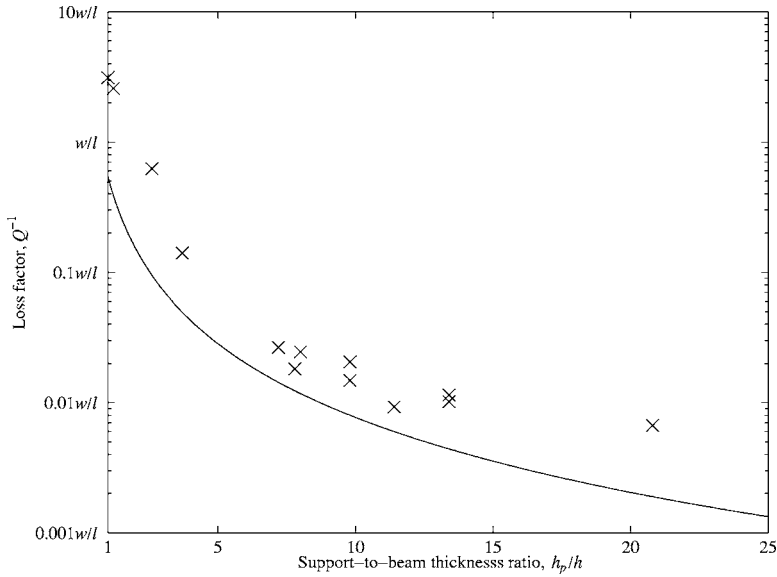


FIG. 5. Measured total cantilever loss factors (×), along with the theoretical prediction for loss factor due to attachment loss (---). Note that the abscissa has a linear scale, unlike the log scale used in Fig. 3.

expected that the data should fall directly on the theoretical curve, since the measurement is one of total  $Q$ , including contributions from other loss mechanisms. The curve in Fig. 5 thus represents a lower bound that measured data would be expected to approach when other loss mechanisms are negligible.

**B. Doubly fixed beams**

**1. Prediction of beam attachment loss**

Attachment loss is calculated in a similar fashion for a beam attached to rigid supports at both ends, referred to variously as a doubly fixed, doubly clamped, or clamped-clamped (“c-c”) beam. The shear force and bending moment developed at the boundaries of such a beam are the same as those given in Eq. (15) and Eq. (16) for a cantilever, except that the coefficient  $\beta_n$  is given by  $[\sin(k_n l) + \sinh(k_n l)] / [\cos(k_n l) - \cosh(k_n l)]$  and the eigenvalues  $k_n l$  are determined from  $\cosh(k_n l) \cos(k_n l) = +1$ . For the fundamental mode of vibration,  $\beta_1 = 0.9825$  and  $k_1 l = 4.730$ . The stored energy of vibration, again  $U_n = 1/2 \rho w h l \omega_n^2 u_0^2$ , is greater than for the cantilever due to the higher resonant frequency  $\omega_n$ .

For a support structure modeled as a half-space, the dominant power flow into the support from the beam attachment point is given by Eq. (6). Since the shear wavelength  $k_s$  in the support is proportional to frequency  $\omega$ , and, for operation at a resonant frequency of the beam,  $\omega = \omega_n$  is proportional to the square of the beam wave number  $k_n$ , the power flow at the attachment point is proportional to  $\beta_n^2 k_n^{10}$ . Furthermore, unlike a cantilever, a doubly fixed beam has two attachment points, so the total flow of power from beam to support must be doubled. Both numerator and denominator of Eq. (14) are greater for a doubly clamped beam than for a cantilever of the same dimensions, the result being that the expression for loss factor in the fundamental mode is the same as in Eq. (17) except that the coefficient  $A$  is a factor of 145.1 higher,

$$A_{c-c} = \frac{2(\beta_1^2 k_1^4)_{c-c}}{(\beta_1^2 k_1^4)_{cant}} A_{cant} = 145.1 A_{cant}. \tag{22}$$

For Poisson’s ratio  $\nu=0.3$ , the coefficient  $A$  is thus 45.0 for loss from a doubly clamped beam into a suitably thick support structure.

For a support modeled as a plate, the power flow given in Eq. (11) is proportional to  $F_s$  and thus to  $\beta_n^2 k_n^6$ , while that given in Eq. (12) is proportional only to  $k_n^6$ , and the cross term in Eq. (13) is proportional to  $\beta_n k_n^6$ . For the fundamental resonant mode, the loss factor again takes the form given in Eq. (18), except that  $A_1$  is greater by a factor of  $2\beta_{c-c}^2 / \beta_{cant}^2$ ,  $A_2$  is greater by a factor of  $2\beta_{c-c} / \beta_{cant}$ , and  $A_3$  is greater by a factor of 2. For  $\nu=0.3$ , the coefficients for a doubly clamped beam are  $A_1=3.40$ ,  $A_2=-1.74$ , and  $A_3=0.48$ .

Figure 6 compares the theoretical predictions of attachment loss for two beams of the same size, one clamped only at one end (a cantilever) and the other clamped at both ends. Both the regime in which the support acts as a plate and the

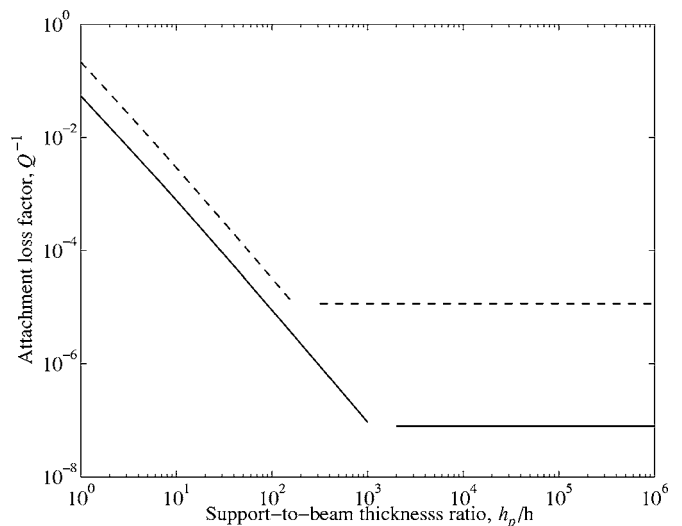


FIG. 6. Comparison of predicted attachment loss from a cantilevered beam resonator (—) and a doubly clamped beam resonator (---) of the same dimensions, each vibrating in its fundamental flexural mode, as a function of ratio of support plate thickness  $h_p$  to beam thickness  $h$ . The curves shown are for the case  $w/l=1/10$  and  $h/l=1/25$ ; all predictions scale linearly with  $w/l$ . Curves are shown for both the plate-model and half-space model of the support.

TABLE II. Geometry, predicted  $Q$ , and measured  $Q$  for doubly fixed beams.

Plate	Beam	Dimensions (mm)			Aspect ratios			Freq. (Hz)	Predictions				Measurements	
		Length $l$	Width $w$	Thickness $h$	$l/w$	$l/h$	$h_p/h$		$Q_{\text{attach}}$	$Q_{\text{visc}}$	$Q_{\text{ac}}$	$Q_{\text{total}}$	Freq. (Hz)	$Q$
1	1	9.53	1.27	0.61	7.5	15.6	20.8	35153	1070	40000	33371	756	28740	1019
	2	19.05	3.84	1.17	5.0	16.3	10.9	16844	201	53000	20332	186	14670	103
	3	12.70	1.78	1.19	7.1	10.6	10.6	38723	278	82000	32419	251	30360	271
2	4	19.05	3.78	1.22	5.0	15.6	7.8	17576	108	57000	22139	104	15130	163
	5	9.53	1.70	0.89	5.6	10.7	10.7	51265	221	70000	125352	205	41000	160
3	6	9.53	1.40	0.74	6.8	13.0	6.5	42251	102	53000	48465	99	33470	53
	7	18.92	2.67	1.35	7.1	14.1	3.5	19669	34	66000	41233	34	18760	19

regime in which the support acts as a half-space are shown. Note that the transition between regimes occurs for thinner support structures in the case of the doubly clamped beam, since the resonant frequency  $\omega$  (and therefore the shear wave number  $k_s$  in the support) is a factor of 6.36 higher than for a cantilever of the same size, and thus the support thickness  $h_p$  that exceeds the shear wavelength is a factor of 6.36 smaller.

## 2. Experimental measurement of doubly fixed beams

Experiments were conducted on seven doubly fixed beams. These beams were fabricated on the same plates as the cantilevers described in Sec. III A, after cantilever measurements were complete. The doubly fixed beams were created by milling a long channel into the interior of the plates (about 70% the length of the plate), leaving only thin bridges spanning the channel. The milled channel was about one-third of the way down from the top so that the beams were near the center of the portion of the plate not buried in sand. The same electrostatic actuation was used to excite the structures, and the same procedures were used to establish the optimal gap between the electrode and beam. As with the cantilevers, measurements of the resonance frequencies and  $Q$  were obtained by sweeping the frequency of the harmonic drive signal and using the half-power bandwidth method.

The measured quality factors are compared to theoretical predictions in Table II. Again, because the measured  $Q$  values are the quality factors due to the combined action of all loss mechanisms, estimates of fluid-related loss mechanisms are included in the table, as well as the total  $Q$ , which includes contributions from attachment loss, viscous and acoustic loss into the surrounding air, and intrinsic loss in the aluminum. The measured values of  $Q$  show the same general trend as the predicted values of  $Q_{\text{total}}$  and are within a factor of 2 for all cases. For all cases except beam #4, the measured values are lower than the predicted values of  $Q_{\text{attach}}$ . The measured data are also shown graphically in Fig. 7 alongside the prediction of attachment loss factor (scaled by aspect ratio  $w/l$ ).

## C. Other oscillator geometries

Other oscillator geometries can be treated in a manner similar to the cantilever and doubly fixed beam. If the oscillator geometry is complicated, the vibration energy in the oscillator and the reaction forces and moments at the point of attachment can be found from numerical models rather than analytical solutions. As an example, we calculate the attachment loss of a rectangular paddle oscillator attached to the substrate by two support arms, as shown in Fig. 8.

Hauke *et al.*<sup>23</sup> present measurements of quality factor,  $Q$ , for such a resonator, in a cryogenic vacuum at temperatures

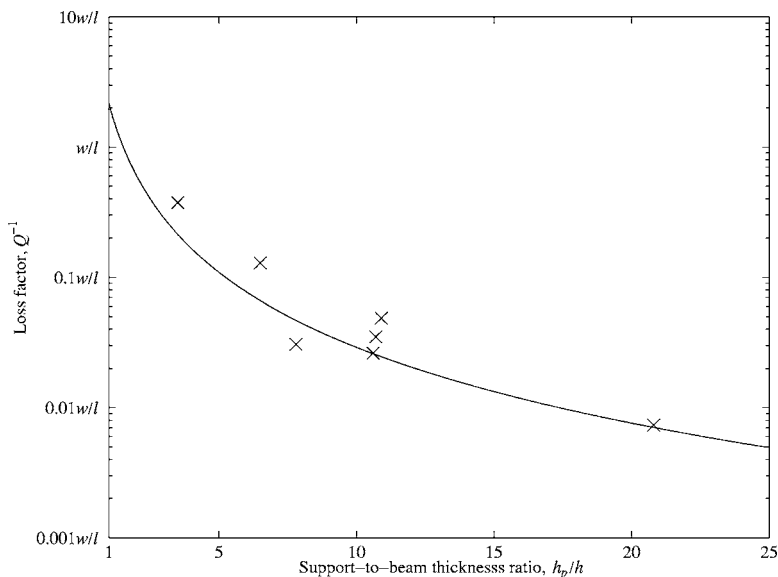


FIG. 7. Measured total loss factors for doubly fixed beams ( $\times$ ), along with the theoretical prediction for loss factor due to attachment loss ( $\text{---}$ ).

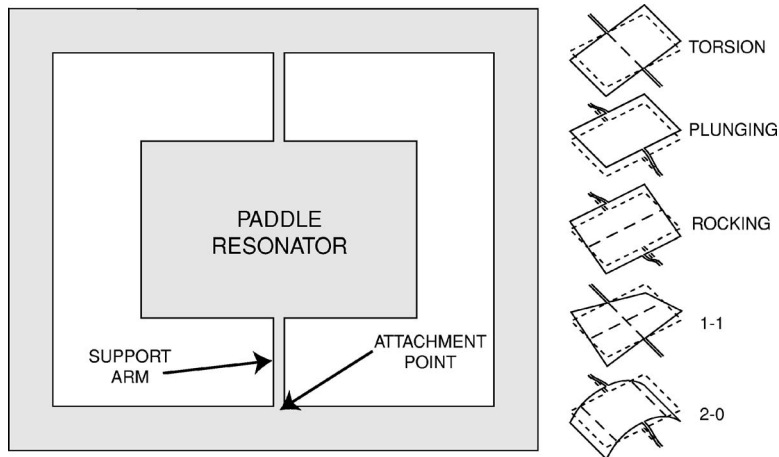


FIG. 8. Rectangular paddle resonator and schematics of first five mode shapes. The resonator and support arms are freestanding and attached to the surrounding structure, which is anchored to the substrate. For the resonator measured by Haucke *et al.* (Ref. 23), the resonator is  $147 \times 97.75 \mu\text{m}$ , and the support arms are  $50.9 \mu\text{m}$  long and  $4.15 \mu\text{m}$  wide.

as low as 15 K. For several of the modes reported, the measured  $Q$ s are insensitive to variations in temperature below 20 K, an indication that temperature-dependent mechanisms such as thermoelastic loss are not the dominant means of energy loss. This suggests that attachment loss, which is insensitive to temperature, may be a significant loss mechanism for this geometry at low temperature, and, indeed, we predict attachment loss to be within an order of magnitude of the measured values.

The displacement of the paddle and support arms in each of the first five modes is available from detailed finite-element simulations. From this, we calculate the shear force  $F_s$  at the intersection of the support arms and the substrate for the second, third, and fifth modes. These modes correspond to rigid out-of-plane translation of the paddle, rotation of the paddle about a nodal line midway between the support arms, and bending of the paddle with two nodal lines in the direction parallel to the support arms, and are referred to as the *plunging*, *rocking*, and *2-0* modes, respectively. The first and fourth modes, characterized, respectively, by rotation of the paddle about the support arms and bending of the paddle with two perpendicular nodal lines, and referred to as the *torsion* and *1-1* modes, involve only torsional motion of the support arms and thus result in no shear force at the point of attachment. In these cases, the torsional moment  $M_t$  applied to the substrate results in predicted attachment loss that is many orders of magnitude less than the measured values reported in Ref. 23.

The paddle was attached to a substrate  $625 \mu\text{m}$  thick, which, although over 400 times thicker than the  $1.5 \mu\text{m}$  thick paddle and support arms, is still only a small fraction of the shear wavelength at the resonant frequencies of the modes in question. The appropriate model for the substrate is thus the plate model of Sec. II B, i.e., power flow into the substrate is obtained via Eq. (11). The vibration energy in the paddle for each mode is also calculated via finite-element analysis, and the loss factor obtained via Eq. (14).

Table III compares the predicted values of  $Q$  to the values measured by Haucke *et al.*<sup>23</sup> at low temperature for modes two, three, and five. In all cases, predicted attachment loss is within an order of magnitude of the total measured loss, indicating that the dominant low-temperature loss mechanism in these modes may be radiation to the support structure.

The differences between the measured and predicted values can be ascribed to a number of causes. Since the experimental values are measurements of *total* loss, while the predictions are only of attachment loss, any other sources of losses present in the experiment cause an increase in the measured loss. This may be the case for the 2-0 mode, for which the predicted attachment loss is just over half of the measured total loss. A second cause of disparity is the assumption made when predicting attachment loss that the substrate is a semi-infinite plate. In reality, the chip upon which the measured paddle was fabricated has overall dimensions of approximately  $1 \times 2 \text{ cm}$ . At the frequency of the 2-0 mode, the bending wavelength in a silicon plate  $625 \mu\text{m}$  thick is  $0.43 \text{ cm}$ , while at the frequency of the plunging mode the wavelength is nearly  $0.9 \text{ cm}$ : the chip dimensions are not significantly greater than the bending wavelength. Thus, the chip is somewhat stiffer (resulting in lower attachment loss) than if it were a semi-infinite plate. It is important to note that if the chip were *smaller* than one bending wavelength, its stiffness with respect to a shear force input would increase rapidly, and the approximation of a semi-infinite support plate would be wholly inappropriate.

#### IV. CONCLUSIONS

Finally, we conclude by comparing the results of the two models of the support structure, and commenting on their utility in various regimes of resonator geometry.

The expressions for power flow given in Sec. II are applicable for any resonator geometry for which the attachment to the support structure acts essentially as a point source for vibration in the support. The plate-support model is appropriate for situations in which a resonator is attached to the edge of a platelike support structure, with thickness that is small compared to the shear wavelength in the material at the

TABLE III. Comparison of predicted and measured loss for a rectangular paddle oscillator.

Mode	Measured frequency	FEM frequency	Measured $Q^{-1}$	Predicted $Q^{-1}$
2 (plunging)	131 kHz	101 kHz	$5 \times 10^{-6}$	$2.5 \times 10^{-5}$
3 (rocking)	265 kHz	281 kHz	$5 \times 10^{-6}$	$1.5 \times 10^{-5}$
5 ("2-0")	536 kHz	542 kHz	$1.2 \times 10^{-6}$	$6.8 \times 10^{-7}$

frequency of operation. Many microscale mechanical resonators fall into this category, typically being fabricated from wafers that are thinner than a few millimeters, and operating at megahertz frequencies at which the shear wavelength is several millimeters or more. In these cases, energy is radiated in the form of flexural waves in the support structure. The semi-infinite-space model of the support provides a good estimate of power flow into supports with thickness that exceeds the shear wavelength. Nanoscale resonators operating near or above 1 GHz will radiate energy into the supporting structure in the form of shear waves with wavelengths on the order of several microns, typically much smaller than the support structure thickness. An intermediate regime, not discussed in this article, will occur in cases in which the support thickness is the same order as the shear wavelength at the frequency of operation. Resonant behavior is possible in cases in which the support thickness matches an small integer number of half-wavelengths; this may be of interest for future investigation since small microscale or large nanoscale resonators may operate in this transition regime.

For the cantilever and doubly clamped beam resonators explored here as case studies, attachment loss was found to scale with the beam width-to-length aspect ratio and with the square of the ratio of beam-to-plate thickness, for a wide range of support structures thicker than the resonator but thin enough to be modeled as a plate. Thus, attachment loss decreases rapidly as the support is stiffened, while, as expected, narrow beams have lower attachment loss than wider beams. For very thick support structures (or very thin beams), the half-space model of the support is appropriate, in which case attachment loss is still directly proportional to beam width-to-length aspect ratio, but is also very strongly dependent on beam thickness-to-length ratio, such that only short, stubby beams will have significant attachment loss.

The macroscale experiments described here provide a validation of the plate-support model for attachment loss, and the comparison of predictions from this model with measurements of microscale paddle oscillators from the existing literature indicates that attachment loss can be the dominant loss mechanism in some circumstances. The half-space-support model predicts very low levels of attachment loss for beamlike resonators, such that other loss mechanisms are likely to dominate for resonators operating in this regime. This three-dimensional half-space-support theory is yet to be validated, but provides a more rigorous estimate of attachment loss than the two-dimensional theory employed previously.

## ACKNOWLEDGMENTS

The authors wish to thank Robert Baden for his translation of Ref. 17 and Martin Marcus for making available the

results of finite-element simulations of the paddle oscillator measured by Haucke *et al.* (Ref. 23). A portion of this work was performed while the first author held a National Research Council Research Associateship Award at the Naval Research Laboratory.

- <sup>1</sup>A. B. Hutchinson, P. Truitt, K. C. Schwab, L. Sekaric, J. M. Parpia, H. G. Craighead, and J. E. Butler, *Appl. Phys. Lett.* **84**, 972 (2004).
- <sup>2</sup>J. Yang, T. Ono, and M. Esashi, *J. Microelectromech. Syst.* **11**, 775 (2002).
- <sup>3</sup>J. Yang, T. Ono, and M. Esashi, *Appl. Phys. Lett.* **77**, 3860 (2000).
- <sup>4</sup>K. Y. Yasumura, T. D. Stowe, E. M. Chow, T. Pfafman, T. W. Kenney, B. C. Stipe, and D. Rugar, *J. Microelectromech. Syst.* **9**, 117 (2000).
- <sup>5</sup>X. Liu, S. F. Morse, J. F. Vignola, D. M. Photiadis, A. S. M. H. Marcus, and B. H. Houston, *Appl. Phys. Lett.* **78**, 1346 (2001).
- <sup>6</sup>L. Lin, R. T. Howe, and A. P. Pisano, *J. Microelectromech. Syst.* **7**, 286 (1998).
- <sup>7</sup>C. T.-C. Nguyen, *IEEE Trans. Microwave Theory Tech.* **47**, 1486 (1999).
- <sup>8</sup>J. A. Judge, B. H. Houston, D. M. Photiadis, and P. C. Herdic, *J. Sound Vib.* **290**, 1119 (2006).
- <sup>9</sup>B. Ilic, H. G. Craighead, S. Krylov, W. Senaratne, C. Ober, and P. Neuzil, *J. Appl. Phys.* **95**, 3694 (2004).
- <sup>10</sup>K. L. Ekinci, X. M. H. Huang, and M. L. Roukes, *Appl. Phys. Lett.* **84**, 4469 (2004).
- <sup>11</sup>A. Gupta, D. Akin, and R. Bashir, *Appl. Phys. Lett.* **84**, 1976 (2004).
- <sup>12</sup>T. R. Albrecht, P. Grütter, D. Horne, and D. Rugar, *J. Appl. Phys.* **69**, 668 (1991).
- <sup>13</sup>T. D. Stowe, K. Yasamura, T. W. Kenny, D. Botkin, K. Wago, and D. Rugar, *Appl. Phys. Lett.* **71**, 288 (1997).
- <sup>14</sup>H. Kawakatsu, S. Kawai, D. Saya, M. Nagashio, D. Kobayashi, H. Toshiyoshi, and H. Fujita, *Rev. Sci. Instrum.* **73**, 2317 (2002).
- <sup>15</sup>K. L. Ekinci and M. L. Roukes, *Rev. Sci. Instrum.* **76**, 061101 (2005).
- <sup>16</sup>Y.-H. Park and K. C. Park, *J. Microelectromech. Syst.* **13**, 238 (2004).
- <sup>17</sup>Y. Jimbo and K. Itao, *J. Horological Inst. Jpn.* 1180-4882 **47**, 1 (1968).
- <sup>18</sup>M. C. Cross and R. Lifshitz, *Phys. Rev. B* **64**, 085324 (2001).
- <sup>19</sup>D. M. Photiadis and J. A. Judge, *Appl. Phys. Lett.* **85**, 482 (2004).
- <sup>20</sup>H. Hosaka, K. Itao, and S. Kuroda, *Sens. Actuators, A* **49**, 87 (1995).
- <sup>21</sup>G. F. Miller and H. Pursey, *Proc. R. Soc. London, Ser. A* **223**, 521 (1954).
- <sup>22</sup>J. Eichler, *J. Acoust. Soc. Am.* **36**, 344 (1964).
- <sup>23</sup>H. Haucke, X. Liu, J. F. Vignola, B. H. Houston, M. H. Marcus, and J. W. Baldwin, *Appl. Phys. Lett.* **86**, 181903 (2005).
- <sup>24</sup>C. R. Fuller, S. J. Elliot, and P. A. Nelson, *Active Control of Vibration* (Academic, San Diego, 1996), p. 29.
- <sup>25</sup>G. N. Bycroft, *Philos. Trans. R. Soc. London, Ser. A* **248**, 327 (1956).
- <sup>26</sup>C. Kauffmann, *J. Acoust. Soc. Am.* **103**, 1874 (1998).
- <sup>27</sup>J. X. Su and A. T. Moorhouse, *J. Acoust. Soc. Am.* **115**, 2075 (2004).
- <sup>28</sup>A. D. Pierce, *Acoustics: An Introduction to its Physical Principles and Applications* (Acoustical Society of America and American Institute of Physics, New York, 1981), p. 122.
- <sup>29</sup>D. J. Inman, *Engineering Vibration*, 2nd ed. (Prentice-Hall, Englewood Cliffs, NJ, 2001).
- <sup>30</sup>S. T. Hansen, A. Turo, F. L. Degertekin, and B. T. Khuri-Yakib, *Proc.-IEEE Ultrason. Symp.*, 947 (2000).
- <sup>31</sup>J. F. Vignola, J. A. Judge, J. Jarzynski, M. Zalalutdinov, B. H. Houston, and J. W. Baldwin, *Appl. Phys. Lett.* **88**, 041921 (2006).
- <sup>32</sup>K. Kokubun, M. Hirata, M. Ono, H. Murekami, and Y. Toda, *J. Vac. Sci. Technol. A* **5**, 2450 (1987).
- <sup>33</sup>K. Kokubun, M. Hirata, M. Ono, H. Murakami, and Y. Toda, *J. Vac. Sci. Technol. A* **3**, 2184 (1985).
- <sup>34</sup>F. R. Blom, S. Bouwstra, M. Elwenspoek, and J. H. J. Fluitman, *J. Vac. Sci. Technol. B* **10**, 19 (1992).
- <sup>35</sup>F. Fahy, *Sound and Structural Vibration: Radiation, Transmission and Response* (Academic, New York, 1985).
- <sup>36</sup>E. G. Williams, *J. Acoust. Soc. Am.* **73**, 1520 (1983).